Progress in Organic Coatings 167 (2022) 106829

Contents lists available at ScienceDirect

Progress in Organic Coatings

journal homepage: www.elsevier.com/locate/porgcoat

Multifunctional coatings based on GNP/epoxy systems: Strain sensing mechanisms and Joule's heating capabilities for de-icing applications

Xoan F. Sánchez-Romate *, Rodrigo Gutiérrez, Alejandro Cortés, Alberto Jiménez-Suárez, Silvia G. Prolongo

Materials Science and Engineering Area, Escuela Superior de Ciencias Experimentales y Tecnología, Universidad Rey Juan Carlos, Calle Tulipán s/n, 28933 Móstoles, Madrid, Spain

ARTICLE INFO

Keywords:
Graphene nanoplatelets
Epoxy
Strain sensing
Joule's heating
de-icing

ABSTRACT

Multifunctional coatings based on a GNP/epoxy system have been manufactured and their strain sensing and Joule's heating capabilities for anti-icing and de-icing applications have been explored. It has been observed that an increase in the GNP content induces a detriment on the gauge factor (from 5.75 at 8% to 2.49 at 12%) due to a lower interparticle distance between nanoparticles, being less sensitive. However, in any case, the GF values at bending conditions are significantly above conventional metallic gauges (which is around 2). On the other hand, the resistive heating is more efficient when increasing the GNP content, as expected, due to a higher number of conducting pathways that allows a more efficient Joule's heating effect. However, and due to the heterogeneity present at 12% GNP samples due to the much higher viscosity of the mixture during the dispersion process, the 10% ones were selected for a de-icing proof of concept, proving that the ice completely melts after 5 min of applying 200 V. Therefore, the proposed GNP coatings show an outstanding capability for both strain sensing and de-icing purposes by resistive heating, being useful for a wide range of applications.

1. Introduction

The development of multifunctional polymeric coatings is now gaining a great deal of attention. More specifically, there are a lot of research in anti-corrosion or anti-fouling coatings, among other applications [1–3].

In this regard, the use of carbon nanoparticles may play a prevalent role due to their exceptional mechanical and physical properties. For example, the use of graphene nanoplatelets and carbon nanotubes has proved to be an efficient way to enhance wear properties due to their lubricant effect, which leads to a reduction in the friction coefficient [4,5].

Apart from the anti-corrosion and wear-enhanced capabilities, it is also particularly interesting some other properties that can be achieved with this type of nanoparticles. More specifically, it is well known that their addition into insulating matrices may enhance their electrical properties. This is explained because they promote the creation of percolating networks, which allows the creation of preferential electrical pathways inside the material [6,7]. In this context, an increase of the electrical conductivity in several orders of magnitude is achieved at very low carbon nanoparticle contents [8–11].

This enhancement of the electrical properties promotes novel functionalities in these polymeric coatings. For example, the inherent piezoresistive response of the carbon nanoparticles, along with their interactions, makes them very suitable for strain sensing applications [12,13]. The basis for their exceptional strain sensing capabilities lies in the fact that there is a prevalence of tunneling mechanisms between neighboring nanoparticles, which plays a dominant role in the electrical properties of the material [14]. The tunneling resistance associated to this effect follows a linear-exponential correlation with applied strain, thus, making them very sensitive [15,16]. In this regard, several studies have proved that the GNP doped composites present a much higher gauge factor (GF) than, for example, the carbon nanotubes (CNTs) doped ones [17,18]. This is explained by the 2D nature of these nanoparticles that allows a higher prevalence of tunneling mechanisms, making them much more sensitive to applied strain, as stated before.

In this context, carbon-doped polymeric coatings have demonstrated not only a huge sensitivity to applied strain but also to damage detection, as it induces an abrupt breakage of the electrical pathways that can be easily detected. In this regard, the development of Electrical

* Corresponding author.
E-mail address: xoan.fernandez.sanchezromate@urjc.es (X.F. Sánchez-Romate).

https://doi.org/10.1016/j.porgcoat.2022.106829
Received 27 October 2021; Received in revised form 10 February 2022; Accepted 16 March 2022
Available online 30 March 2022

Impedance Tomography (EIT) techniques allows the creation of damage mapping by electrical resistance measurements in simultaneous channels [19,20]. On the other hand, GNP-based polymeric coatings have demonstrated excellent strain sensing properties under bending and tensile and compressive strain which can be easily modelled depending on the different interactions among nanoparticles [21,22]. In addition, some research explored the effect of abrasion in the electrical conductivity of carbon nanofiber and Ag nanoparticle-based polymers, showing a slight reduction of the electrical conductivity with the increasing abrasion cycles [23,24], proving the high electromechanical sensitivity of this type of nanocomposites. Therefore, their use in a wide range of Structural Health Monitoring (SHM) applications is now gaining a lot of interest, such as wearable sensors for human motion monitoring [25–27].

Apart from SHM purposes, the enhancement of the electrical properties opens other functionalities such as the resistive heating, taking advantage of Joule's heating effect. In this regard, the heat flow in a sample, Q, is proportional to the applied voltage, V, the current going through the sample, I, and the time the voltage is applied, t, following the well-known Joule's formula:

$$Q = V \bullet I \bullet t \quad (1)$$

Joule's heating capabilities have been explored for the development of deicing systems. More specifically, temperature increments of 40 °C have been achieved with relatively low GNP contents (8 to 12 wt%), enough for an efficient deicing [28],whereas increments of around 20 °C in polyurethane coatings with 8 wt% GNP [29]. Similar results with higher temperature increments were also observed with printed circuits made of low CNT contents over a glass fiber substrate [30,31].

In addition, the good barrier properties of GNPs promote a detriment on the wettability of these polymeric coating that can be useful for anti-icing applications. For example, the addition of relative low GNP contents promotes a prevalent increase of the contact angle of a water droplet [32]. Therefore, the addition of GNPs to polymeric coatings has demonstrated to be an efficient way to achieve proper anti-icing and deicing systems (ADIS). In addition, the presence of other type of nanoparticles, such as Ag, have been proved to give superhydrophobic properties, leading to contact angles of above 150° [33,34]. A similar fact was observed in textile materials with the addition of MXene nanosheets [24].

This study aims to develop easily manufactured and scalable multifunctional GNP-based polymeric coatings. More specifically, the strain sensitivity to bending strain is explored as a function of the GNP content and their Joule's heating capabilities are evaluated whereas their effect on the adhesion strength of the coating to the glass fiber substrate is also explored. Finally, a proof of concept of deicing is carried out by means of resistive heating. By this way, these nanostructured polymeric coatings could be used for multiple applications by reducing the maintenance costs due to their strain sensing capabilities and the problems associated to the ice formation by deicing via Joule's resistive heating.

2. Materials and methods

2.1. Materials

The nanoparticles used in this study were GNPs with a commercial name *M25*, supplied by *XGSciences*. They have an average lateral size of 25 μm and a thickness around 6–10 nm.

The resin was an epoxy-based one, *Bisphenol A diglycidyl ether (DGEBA)*, with an amino hardener, *Triethylenetetramine (TETA)*, supplied by *Sigma Aldrich*. The mass proportion monomer to hardener is 100 to 14.3.

The substrates were made of glass fiber (GFRP), supplied by *Rochling*, with the commercial name of *Durostone EPC 203*. It has a peel-ply surface treatment to guarantee a proper adhesion between the coating and the substrate.

2.2. Manufacturing of GNP/epoxy coatings

The manufacturing of GNP/epoxy coatings were carried out in three phases: 1) Mechanical dispersion of the GNPs into the epoxy mixture, 2) application of the mixture over the GFRP substrate and 3) curing of the coatings.

GNP dispersion was carried out by means of three roll milling. In this regard, it was previously observed for a similar system in another study that the application of a single three roll milling cycle at a 250 rpm rotating speed and a gap distance between the rolls of 120 and 40 μm was enough to ensure a high value of electrical conductivity as the GNPs are not severely damaged [35]. Prior to three roll milling process, the GNPs were manually mixed into the epoxy resin and the mixture was heated up to 45 °C to diminish the viscosity.

After the dispersion procedure, the resulting GNP mixture was degasified at 60 °C under vacuum conditions and the hardener was added in a stoichiometric ratio. Then, it was applied over the GFRP substrate using a coater *ELCOMETER 4340* with a thickness of around 400 μm.

Finally, the mixtures were cured in a conventional oven for 3 h at 60 °C, in order to obtain the final coatings.

2.3. Structural characterization

A microstructural analysis was carried out by means of SEM, using a *Hitachi S4000* apparatus, supplied by *Hitachi*. For this purpose, transversal sections of GNP coatings were cut and polished for a proper observation.

Moreover, the adhesion capabilities were also characterized by means of pull-off tests using a metallic pin and *DeFelsko Automatic Adhesion Tester* device. The metallic pins were bonded to the coating surface by using an epoxy adhesive *LOCTITE EA 9466* with a curing cycle of 24 h at room temperature.

2.4. Electrical conductivity characterization

The electrical conductivity of the coatings was measured by using a Source Meter Unit (Keithley 2410). It was estimated by the slope of I-V curves in a range of 0–10 V for three specimens of each condition. The samples were 100 × 20 mm, with a thickness of the coating ranging from 400 to 500 μm.

2.5. Strain sensing and Joule's heating tests

Strain sensing capabilities were explored in the GNP coatings under bending conditions. In this regard, the electrical resistance was measured during the mechanical test by using an *Agilent 34410A* module. The electrical resistance was measured under compressive and tensile conditions in the bending tests between two copper wires attached with silver ink (Fig. 1a). The test rate was set at 1 mm/min and the electrical properties were measured under consecutive load cycles up to 1% strain.

Joule's heating capabilities were carried out by applying an external voltage between two copper electrodes in samples of 100 × 20 mm, as shown in the schematics of Fig. 1b. The voltage was applied by using a *Keithley 2410* power source and temperature was measured with an infrared thermographic camera *FLIR E50*.

Finally, de-icing capabilities of GNP coatings under Joule's heating were also investigated. In this regard, an ice sheet of 2 mm thickness was placed in the central region of a 150 × 150 mm sample, and two conditions were tested: on one hand, without applying an external voltage (reference sample) and, on the other hand, by applying an external voltage of 200 V (Fig. 1c). The temperature was measured during the test by using the IR camera described before.

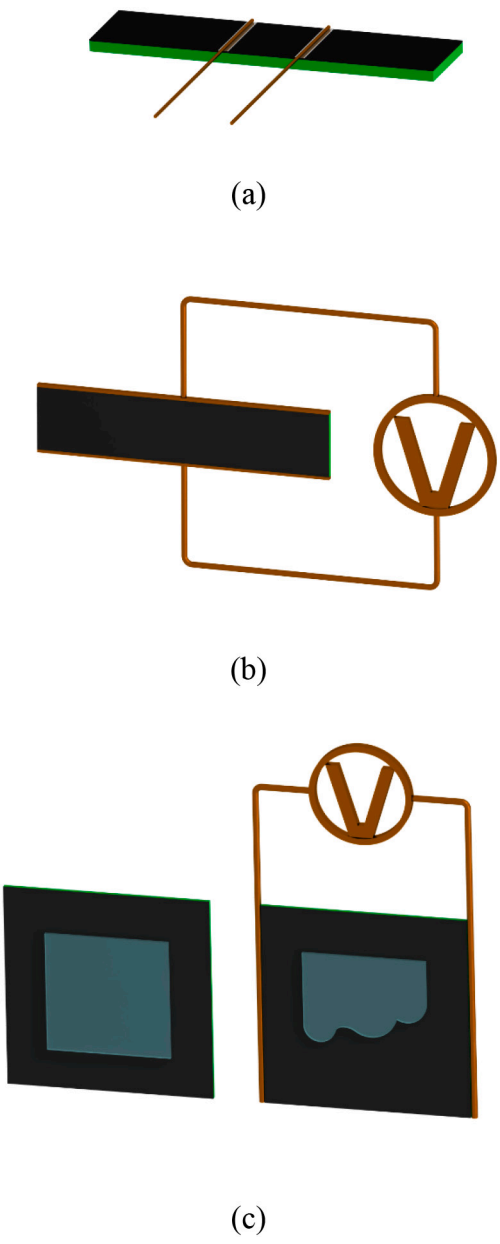

Fig. 1. Schematics of (a) strain sensing tests, (b), Joule's heating characterization and (c) de-icing tests where the ice melting is observed in the sample connected to a power supply.

3. Results and discussion

First, a characterization of the GNP-reinforced polymeric coatings is carried out under SEM analysis, followed by Joule's heating and strain sensing tests. Then, a proof of concept of a deicing application is carried out to prove the applicability of the developed coatings.

3.1. Microstructural characterization

Fig. 2 shows SEM images of the transversal section of the GNP coatings for the different conditions. Here, it can be observed that, by increasing the GNP content, the porosity is increased, as observed when comparing Fig. 2a and e, corresponding to 8 and 12% GNP samples, respectively. This is explained because of the increasing viscosity of the GNP/epoxy mixture, that induces a poor degasification, being more difficult to remove the entrapped air. Moreover, this increasing viscosity also promotes a poor wettability of the epoxy mixture to the substrate surface. In this regard, Table 1 summarizes the values of the adhesion strength for the different conditions. It can be observed that the maximum value is achieved at 8% GNP whereas the coating with 12% GNP presents a significantly lower adhesion strength due to the creation of the previously mentioned weak interfaces between coating and substrate. Nevertheless, despite the lower adhesion strength values, the quality of the coating is relatively high as the presence of porosity or weak interfaces is not very prevalent.

Concerning the GNP distribution, the red arrows of Fig. 2b, d and f denote the presence of GNPs inside the epoxy coating. It can be observed that there is no prevalent aggregation of nanoparticles regardless the GNP content, indicating that the dispersion procedure carried out is optimal to achieve a good distribution of nanoparticles.

In this regard, Fig. 3 shows some images of the coatings and the pins after the adhesion test. It can be observed that the failure mode changes from mixed at 8% GNP (Fig. 3a), to mainly adhesive at 10% GNP (Fig. 3b) and, finally, to only adhesive at 12% GNP (Fig. 3c), which explains the lower values of the adhesion strength obtained. Therefore, it can be concluded that, in terms of morphology, higher amounts of nanoparticles would lead to less-quality coatings, by inducing defects on the interface, as well as higher heterogeneities in the coatings themselves.

3.2. Joule's heating capabilities

Although the increasing number of nanoparticles could lead to coatings with a more irregular morphology and higher presence of defects, it is necessary to further explore their functionalities to select the optimum nanoparticle content depending on the application.

For this purpose, Fig. 4a summarizes the electrical conductivity values for each condition. It has been observed that by increasing the GNP content, there is a significant increase of the electrical conductivity from 0.3 at 8 wt% to 18 S/m at 12 wt%. The values are significantly higher than those obtained for a similar system in bulk nanocomposites [18]. This can be explained by the higher 2D disposition of the GNPs in the coatings, leading to a higher efficiency of the electrical pathways. In addition, the results are in good agreement with the GNP distribution observed in the SEM images of Fig. 2, indicating that the dispersion is good enough to generate efficient electrical pathways inside the epoxy coating. Furthermore, the I-V curves of the samples (Fig. 4b to d) show a linear correlation between the current and the voltage, that is, the samples present an ohmic behavior.

In this context, Fig. 5 shows the temperature reached as a function of the voltage applied during Joule's heating tests.

When comparing the different conditions, it can be noticed that, by increasing the nanoparticle content, the resistive heating capabilities are improved. More specifically, the 8 wt% GNP coatings reach an average temperature of around 100 °C at 100 V, whereas the 10 and 12 wt% GNP ones reach a similar mean temperature at 35 and 15 V, respectively.

This enhancement of the resistive heating with increasing the GNP content has been widely reported in other studies with other GNP-epoxy systems [18,28], and it is correlated to the enhanced electrical conductivity. In this regard, by increasing the GNP content, the number of preferential electrical pathways is also increased and, thus, the current flow during the resistive heating, leading to a higher heat flow, as stated in Eq. (1).

Furthermore, when comparing to other similar studies (Table 2), it can be observed that the temperature reached in the samples with the applied voltage is quite high, a fact that is explained, as commented before, by the high electrical conductivity achieved in the samples due to the effectiveness of the dispersion procedure that allows a proper distribution of the GNPs inside the epoxy matrix. Therefore, the proposed GNP/epoxy coating are a promising solution for applications that required good resistive heating properties.

Apart from the temperature reached in the samples, another crucial factor is the homogeneity of the heating. In this regard, from the

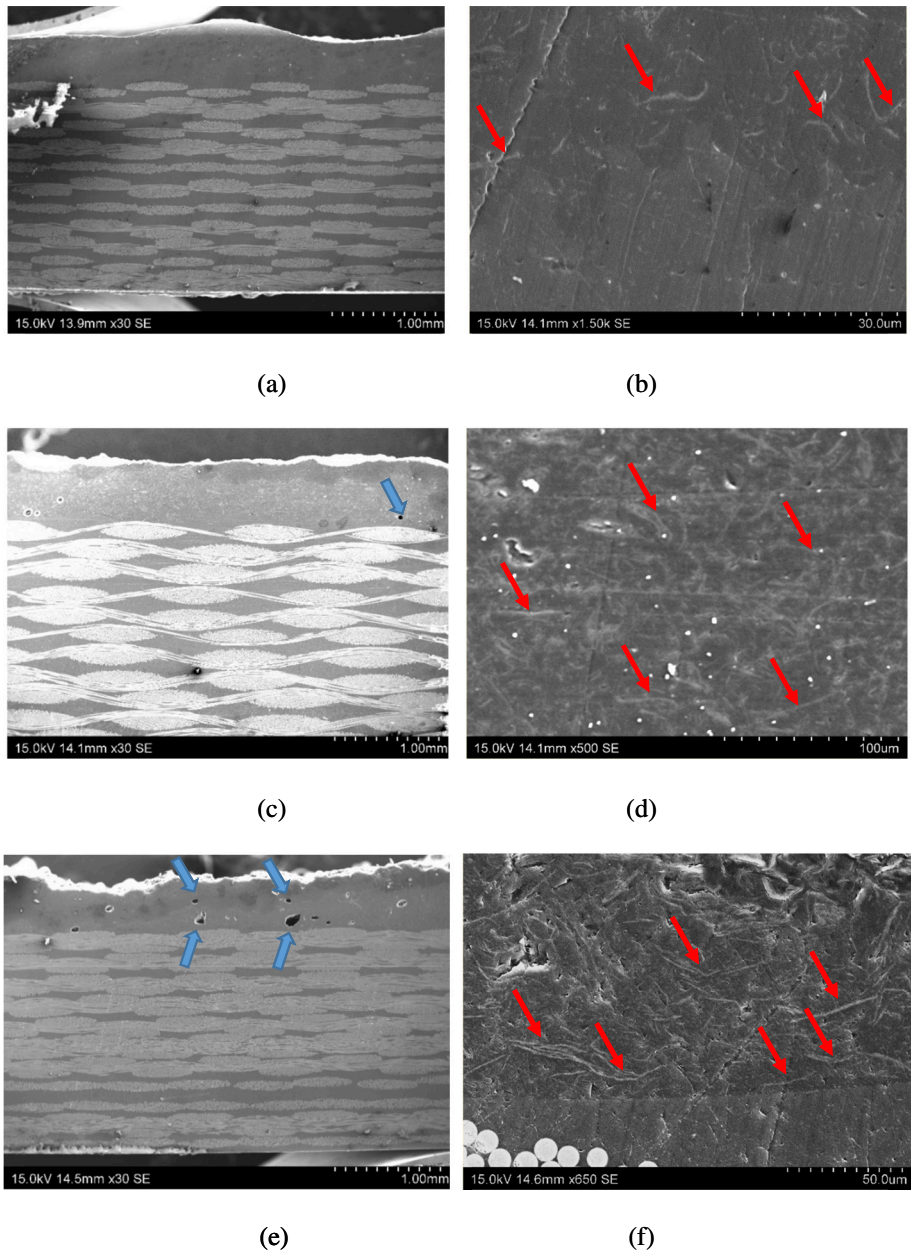

Fig. 2. SEM images of transversal sections of (a-b) 8, (c-d), 10 and (e-f) 12 wt% GNP coatings where the blue arrows denote the presence of prevalent porosity and red arrows denote the GNP distribution in the coatings. (For interpretation of the references to colour in this figure legend, the reader is referred to the web version of this article.)

Table 1
Adhesion strength values for the different coatings.

wt% GNP	Adhesion strength (MPa)
8	7.95 ± 0.67
10	7.91 ± 0.93
12	6.49 ± 1.11

temperature profiles obtained by the IR images, it can be observed that the resistive heating is more homogeneous in the samples with lower GNP contents, with no significant differences between the maximum and the average temperature achieved. However, when increasing the GNP content, the heterogeneity of the heating is also increased, as it can be observed when comparing the average and the maximum temperatures reached in the samples and shown in Fig. 5. Here, it can be noticed that the samples with 8% GNP present a deviation of 10 °C between the average and the maximum temperature at 120 °C whereas this deviation increases up to 15 °C in the samples with 12% wt. GNP. This is explained by the inherent heterogeneity of the coating, as stated before, which presents a higher presence of porosity and an irregular morphology, in combination with the presence of weak interfaces, leading to a heterogeneous distribution of the preferential electrical pathways, and, thus, to a more heterogeneous heating of the sample.

Therefore, from heating tests, it can be stated that, although the 12% GNP samples present the best Joule's resistive capabilities, the heterogeneity observed in these coatings could lead to an inefficient de-icing effect due to a heterogeneous heating of the samples, being a crucial factor to be considered for this type of applications.

3.3. Strain monitoring tests

Once Joule's heating capability has been analyzed, it is important to

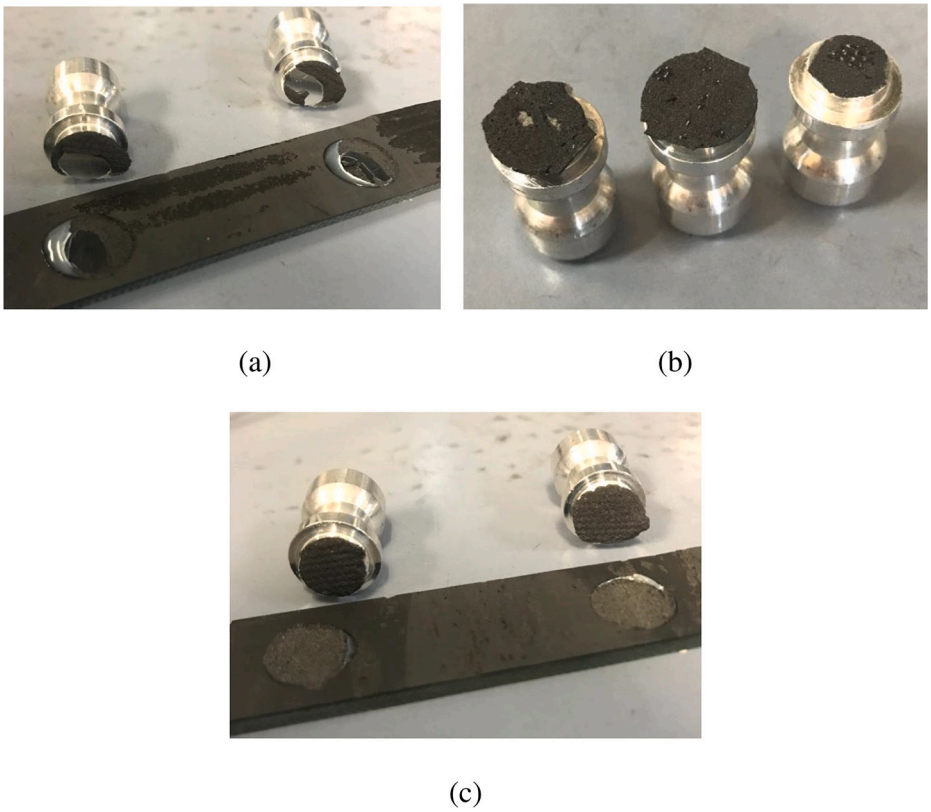

Fig. 3. Images of the adhesion tests of (a) 8, (b) 10 and (c) 12 wt% GNP coatings.

explore other crucial functionality, that is the use of these coatings as strain sensors. In this context, Table 3 summarizes the values of the GF for the different conditions during the bending tests at a tensile and at a compressive subjected face. Here, several facts can be stated. On one hand, the GF values decrease with increasing the GNP content. This is explained by the effect of the tunneling resistance in the strain sensing capabilities of these sensors. By increasing the GNP content, the number of electrical pathways is also increased and, thus, the tunneling distance between neighboring nanoparticles is decreased and the prevalence of preferential pathways throughout the aggregates is also higher. Since the tunneling resistance, which is the main conducting mechanism dominating the electromechanical behavior of this type of nanocomposites, follows a linear-exponential law with the tunneling distance, the electromechanical sensitivity, thus, would decrease with decreasing the interparticle distance. In fact, these results are in total agreement with most of studies dealing with this type of sensors [18,39].

This detriment of the GF is observed for both tensile and compressive subjected faces during the bending tests. However, at tensile conditions, the variations with GNP content are more prevalent. This is explained because at compressive conditions, not only the tunneling resistance plays a prevalent role but also the presence of possible local buckling mechanisms between adjacent GNPs [22].

Furthermore, it can be observed that GF at tensile conditions is significantly higher than at compressive load. This effect can be explored in previous studies [21,22] and it is correlated to the strain mechanisms at compressive loading. Here, the out-of-plane mechanisms play a significant role, as it induces a decrease of the tunneling resistance due to Poisson effect. Therefore, it affects the GF calculated at compressive conditions, which is quite below that obtained at tensile conditions.

Furthermore, apart from the electrical sensitivity, it is important to characterize the repeatability of the strain monitoring mechanisms. For this reason, the sensors were subjected to cycling bending tests. In this regard, Fig. 6 shows the results of the electrical resistance under consecutive load cycles.

First, it can be noticed that the electrical resistance increases when applying the load in the tensile face, whereas a decrease is observed in the compressive one, as the tunneling distance between neighboring particles is reduced. Therefore, the sensors allow to distinguish among the different load applied by revealing a different electrical response.

Moreover, it can be observed that the tensile-subjected face shows a very stable response (Fig. 6a) under consecutive cycles, with no prevalent differences in terms of sensitivity, as well as similar baseline electrical resistance values. In case of compressive-subjected face, however, some differences between the electrical response in consecutive cycles can be noticed (Fig. 6b). More specifically, it can be observed that the electrical sensitivity generally increases with increasing the number of load cycles. This can be correlated to the intrinsic irreversibility of the GNP network once deformed for the first time, that has been reported previously in other studies [40]. This irreversibility explains the fact that the electrical network is not totally recovered once deformed and, thus, the electrical sensitivity could change in consecutive cycles until reaching a stable behavior. In case of compressive loads, it is easier that the electrical network presents this irreversible behavior due to the presence of possible local buckling effects or inherent reversibility of the GNP network, as commented before. The fact that the electrical resistance is recovered in each cycle after application of the load denotes that the sensors are not damaged at a macroscopic level, so they can be used for the monitoring of cycling load under this level of mechanical strain.

Therefore, based on the results of the strain monitoring tests, it can be concluded that the proposed GNP coatings can be used for detection of small strains with a high robustness. In addition, it is important to mention that, even at bending condition, the GF values are quite above those obtained for conventional metallic gauges (usually around 2), specially at low GNP contents.

3.4. De-icing test

The Joule's heating and strain sensing capabilities, jointly with the

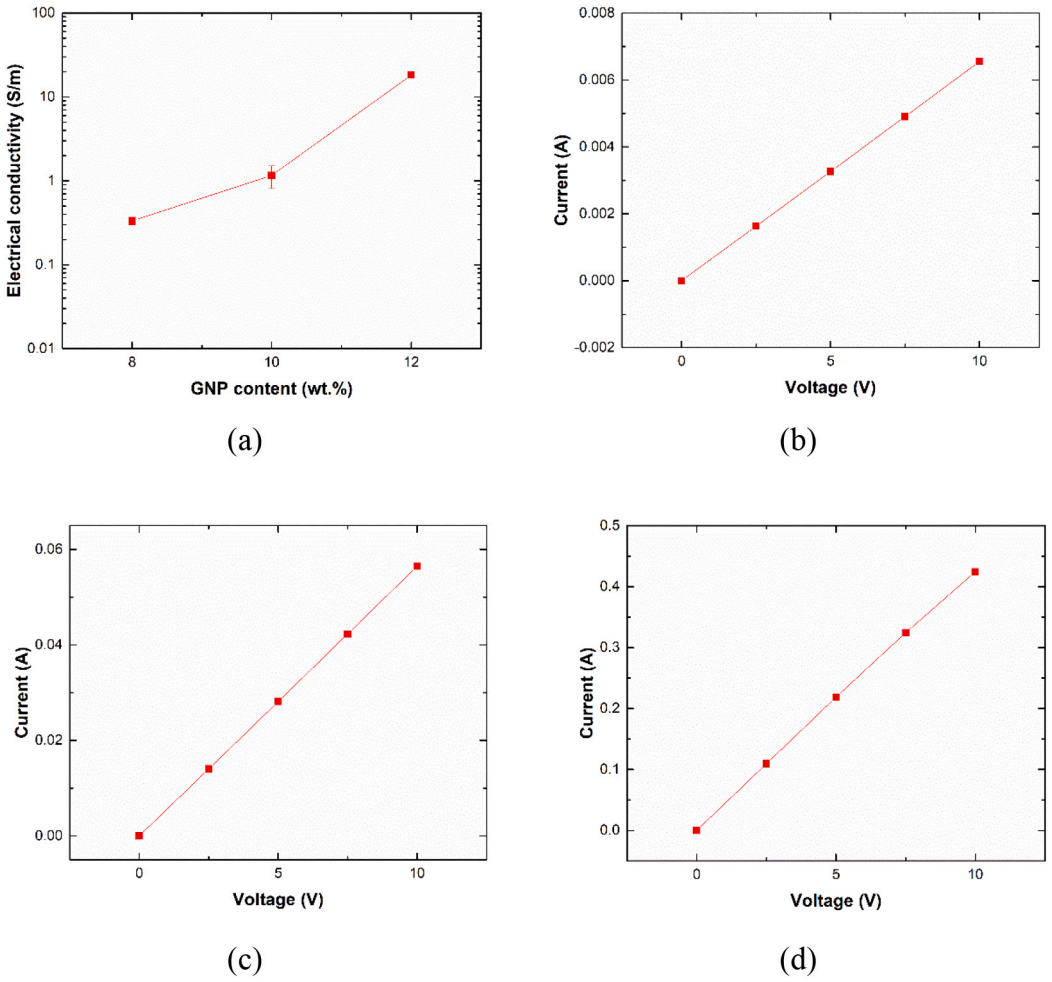

Fig. 4. (a) Electrical conductivity measurements of the coatings and I-V curves of (b) 8, (c) 10 and (d) 12 wt% samples.

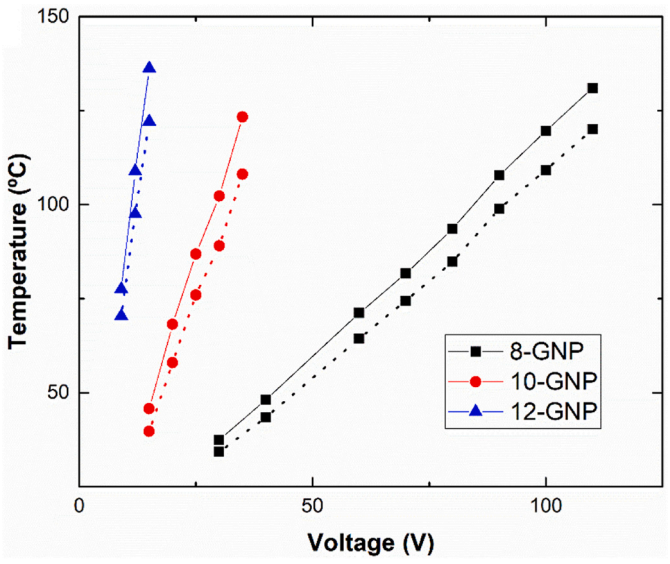

Fig. 5. Temperature reached as a function of applied voltage for the different conditions where the solid lines denote the maximum and the dashed lines the average temperature throughout the coating.

Table 2
Results of the Joule's heating capabilities of this study and other similar research.

Condition	T (°C) and Voltage (V) applied	Reference
10% GNP/epoxy	110 °C and 30 V	This work
10% GNP/epoxy	50 °C and 800 V	[28]
8% GNP/epoxy	140 °C and 100 V (bulk)	[18]
0.5% rGO/epoxy	60 °C and 240 V (bulk)	[36]
5% Graphene nanoribbons/epoxy	100 °C and 30 V	[37]
8% graphene/polyester fabric	70 °C and 50 V	[38]

Table 3
GF values obtained for the different conditions during the bending tests.

Condition	GF (tensile)	GF (compressive)
8% GNP	5.75 ± 0.14	2.51 ± 0.16
10% GNP	3.73 ± 0.10	1.60 ± 0.24
12% GNP	2.49 ± 0.07	1.59 ± 0.07

analysis of the morphology of the GNP coatings, reveal that, although the coatings with 12% GNP present the best resistive heating properties, they also have an irregular morphology, with the presence of prevalent heterogeneities. In addition, they also present the lowest GF values for strain sensing purposes. Therefore, it can be stated that 10% GNP samples present the best balance among functionalities, as they allow an efficient and homogeneous resistive heating without significantly affect the electromechanical properties. For this reason, the 10% GNP content

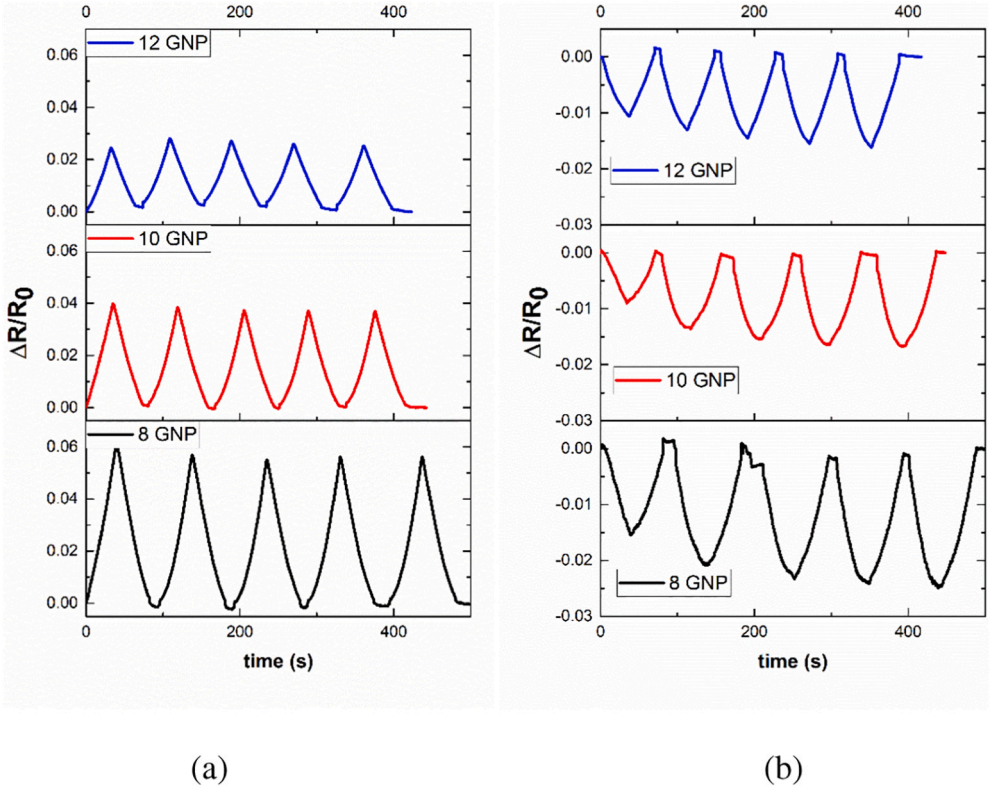

Fig. 6. Electromechanical response on consecutive cycles on bending tests in (a) tensile-subjected and (b) compressive-subjected face.

was selected to evaluate the de-icing capabilities of the GNP/epoxy coatings. This sample was compared to a reference one, without application of external voltage, to highlight the potential for this kind of applications.

In this regard, Fig. 7 shows the temperature profile during the de-icing test in the region where the ice is initially located (highlighted in red in Fig. 7b). Here, several facts can be stated. On one hand, there is a monotonically increase of the average temperature in the central region of the sample that is associated to the gradual melting of the ice.

On the other hand, when looking at the minimum temperature profile, two regions can be observed: 1) a plateau region which corresponds to the solid-liquid phase transformation of the water, that is initially below 0 °C and 2) a final drastic increase once the ice is melted, where the minimum temperature is above 0 °C.

Here, it is important to point out that the minimum temperature is the best parameter to know if there is remaining ice over the sample, although the average temperature offers a global overview about the effectiveness of the resistive heating for the de-icing purpose. This minimum temperature, as can be observed in the IR images of Fig. 7b to e is located in the center of the sample, as the ice melting starts in the external regions and progressively propagates through the central region. In this regard, a complete ice removal is achieved in the sample at 5 min, just when the minimum temperature starts to increase above 0° (third stage of the temperature profile).

Finally, when comparing these results to the reference (undoped) sample, it can be stated that this one does not present any significant temperature increase, as expected, and, therefore, the ice is not removed by the time it is melted in the doped ones, as observed in the IR images of Fig. 7b to e and the photographs of the set-up (Fig. 7f and g). Therefore, it can be said that the proposed GNP coatings present a promising applicability also for de-icing purposes by resistive heating. In this regard, several solutions are based in the use of superhydrophobic coatings to avoid the ice accumulation, by using salt or ionic compounds [41]. With the proposed coating, a high multifunctionality would be achieved by combining the strain sensing characteristics, that would give useful information about the health of the coating and a good de-icing system by resistive heating.

4. Conclusions

In this study, the strain sensing and Joule's heating capabilities for SHM and de-icing applications of GNP coatings have been explored.

It has been observed that, from the microstructural point of view, an increase of the GNP content leads to a more heterogeneous material with a more prevalence of porosities, promoting the creation of lower-quality coatings. More specifically, the values of the adhesion strength present a detriment of around 20% from 8 to 12 wt% samples.

Strain sensing tests prove a good repeatability of the electromechanical response under consecutive cycles on the tensile-subjected face during bending tests. However, some irreversibility is found in the first load cycles on the compressive-subjected face. It is explained by some inherent irreversibility of the GNP network at compressive conditions. In this case, an increase of the GNP content leads to a reduction of the sensitivity, due to a lower prevalence of the tunneling mechanisms.

Joule's heating capability shows that an increase nanofiller content promotes a more efficient resistive heating, as it is mainly influence by the electrical conductivity of the mixture. However, the coatings with higher GNP contents also showed the most heterogenous heating due to the more prevalent presence of defects.

Finally, a proof of concept of de-icing capabilities was carried out. It was stated that ice is completely melted at 5 min of applying the external voltage, leading to an efficient icing removal.

Therefore, the proposed GNP coatings showed very good strain sensing and Joule's heating capabilities, making them a very promising solution for SHM and de-icing applications.

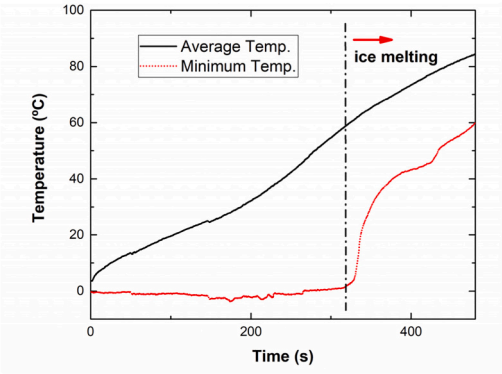

(a)

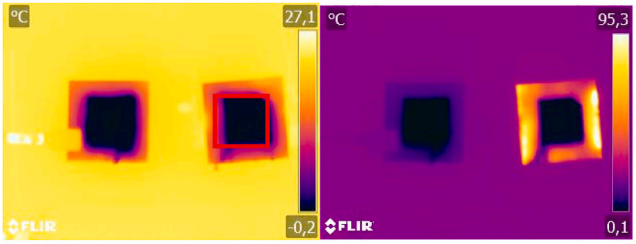

(b) (c)

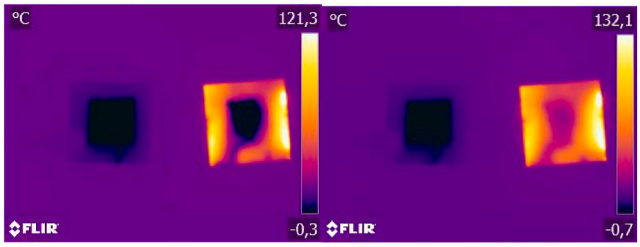

(d) (e)

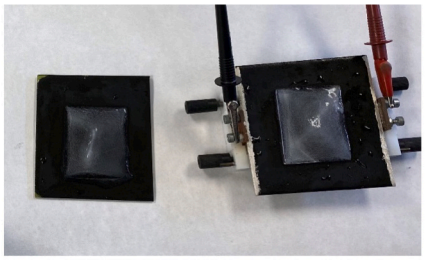

(f)

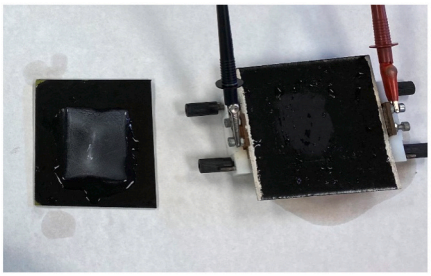

(g)

Fig. 7. (a) Temperature profile during de-icing tests, IR images at (b) initial state and after (c) 2 min, (d) 4 min and (e) 6 min of volatge application and photographs showing (f) the initial state and (g) complete de-icing after Joule's heating test (the left specimen corresponds to the reference coating and the right one to the Joule's heated).

CRediT authorship contribution statement

Xoan F. Sánchez-Romate: Conceptualization, Methodology, Formal analysis, Writing – original draft. **Rodrigo Gutiérrez:** Methodology, Formal analysis. **Alejandro Cortés:** Methodology, Writing – review & editing. **Alberto Jiménez-Suárez:** Conceptualization, Methodology, Funding acquisition, Writing – review & editing. **Silvia G. Prolongo:** Supervision, Funding acquisition.

Declaration of competing interest

The authors declare that they have no known competing financial interests or personal relationships that could have appeared to influence the work reported in this paper.

Acknowledgements

This work was supported by the Ministerio de Economía y Competitividad of Spanish Government [PROJECT PID2019-106703RB-I00], Comunidad de Madrid regional government [PROJECT ADITIMAT-CM (S2018/NMT-4411)] and Young Researchers R&D Project [Ref. M2183, SMART-MULTICOAT] funded by Universidad Rey Juan Carlos and Comunidad de Madrid.

References

[1] André Duarte B.L. Ferreira, P.R.O. Nóvoa, A.T. Marques, Multifunctional material systems: a state-of-the-art review, Compos. Struct. 151 (2016) 3–35.
[2] Thom Nguyen Thi, Thanh Dinh Thi Mai, Nam Pham Thi, Phuong Nguyen Thu, Van Vu Thi Hai, Minh Ngo Quang, Enhanced anti-corrosion protection of carbon steel with silica-polypyrrole-dodecyl sulfate incorporated into epoxy coating, J. Electron. Mater. 48 (2019) 3931–3938.
[3] N.H. Othman, M.C. Ismail, M. Mustapha, N. Sallih, K.E. Kee, R.A. Jaal, Graphene-based polymer nanocomposites as barrier coatings for corrosion protection, Prog. Org. Coat. 135 (2019) 82–99.
[4] W. Zhang, G.J. Ma, C.W. Wu, Anti-friction, wear-proof and self-lubrication application of carbon nanotubes, Rev. Adv. Mater. Sci. 36 (2014) 75–88.
[5] X. Chen, S. Lu, C. Sun, Z. Song, J. Kang, Y. Cao, Exploring impacts of hyper-branched polyester surface modification of graphene oxide on the mechanical performances of acrylonitrile-butadiene-styrene, Polymers. 13 (2021) 2614.
[6] X.F. Sánchez-Romate, A. Jiménez-Suárez, M. Sánchez, A. Güemes, A. Ureña, Novel approach to percolation threshold on electrical conductivity of carbon nanotube reinforced nanocomposites, RSC Adv. 6 (2016) 43418–43428.
[7] S.G. Prolongo, R. Moriche, A. Urena, S. Florez, I. Gaztelumendi, C. Arribas, M. G. Prolongo, Carbon nanotubes and graphene into thermosetting composites: synergy and combined effect, J. Appl. Polym. Sci. 135 (2018) 46475.
[8] M.B. Bryning, M.F. Islam, J.M. Kikkawa, A.G. Yodh, Very low conductivity threshold in bulk isotropic single-walled carbon nanotube–epoxy composites, Adv. Mater. 17 (2005) 1186–1191.
[9] V. Rezazadeh, M.R. Pourhossaini, A. Salimi, Effect of amine-functionalized dispersant on cure and electrical properties of carbon nanotube/epoxy nanocomposites, Prog. Org. Coat. 111 (2017) 389–394.
[10] G. Sun, S. Zhang, Z. Yang, J. Wang, R. Chen, L. Sun, Z. Yang, S. Han, Fabrication and mechanical, electrical properties study of isocyanate-based polyimide films modified by reduced graphene oxide, Prog. Org. Coat. 143 (2020) 105611.
[11] X.F. Sánchez-Romate, A. Jiménez-Suárez, M. Campo, A. Ureña, S.G. Prolongo, Electrical properties and strain sensing mechanisms in hybrid graphene nanoplatelet/carbon nanotube nanocomposites, Sensors. 21 (2021) 5530.
[12] A. Güemes, A.R. Pozo Morales, A. Fernandez-Lopez, X.X.F. Sanchez-Romate, M. Sanchez, A. Ureña, Directional response of randomly dispersed carbon nanotube strain sensors, Sensors. 20 (2020) 2980.
[13] Y. Ko, J. Kim, C.C. Vu, J. Kim, Ultrasensitive strain sensor based on pre-generated crack networks using ag nanoparticles/single-walled carbon nanotube (SWCNT) hybrid fillers and a polyester woven elastic band, Sensors. 21 (2021) 2531.
[14] C. Li, E.T. Thostenson, T. Chou, Dominant role of tunneling resistance in the electrical conductivity of carbon nanotube–based composites, Appl. Phys. Lett. 91 (2007) 223114.
[15] J.G. Simmons, Generalized formula for the electric tunnel effect between similar electrodes separated by a thin insulating film, J. Appl. Phys. 34 (1963) 1793–1803.
[16] N. Hu, Y. Karube, M. Arai, T. Watanabe, C. Yan, Y. Li, Y. Liu, H. Fukunaga, Investigation on sensitivity of a polymer/carbon nanotube composite strain sensor, Carbon 48 (2010) 680–687.
[17] X.F. Sánchez-Romate, J. Artigas, A. Jiménez-Suárez, M. Sánchez, A. Güemes, A. Ureña, Critical parameters of carbon nanotube reinforced composites for structural health monitoring applications: empirical results versus theoretical predictions, Compos. Sci. Technol. 171 (2019) 44–53.

[18] X.F. Sánchez-Romate, A. Sans, A. Jiménez-Suárez, M. Campo, A. Ureña, S. G. Prolongo, Highly multifunctional GNP/epoxy nanocomposites: from strain-sensing to joule heating applications, Nanomaterials 10 (2020) 2431.
[19] K.J. Loh, T. Hou, J.P. Lynch, N.A. Kotov, Carbon nanotube sensing skins for spatial strain and impact damage identification, J. Nondestruct. Eval. 28 (2009) 9–25.
[20] T.N. Tallman, S. Gungor, K.W. Wang, C.E. Bakis, Tactile imaging and distributed strain sensing in highly flexible carbon nanofiber/polyurethane nanocomposites, Carbon 95 (2015) 485–493.
[21] M. Sánchez, R. Moriche, X.F. Sánchez-Romate, S.G. Prolongo, J. Rams, A. Ureña, Effect of graphene nanoplatelets thickness on strain sensitivity of nanocomposites: a deeper theoretical to experimental analysis, Compos. Sci. Technol. 181 (2019) 107697.
[22] X.F. Sánchez-Romate, R. Moriche, A. Jiménez-Suárez, M. Sánchez, S.G. Prolongo, A. Ureña, Sensitive response of GNP/epoxy coatings as strain sensors: analysis of tensile-compressive and reversible cyclic behavior, Smart Mater. Struct. 29 (2020), 065012.
[23] L. Zhang, J. Luo, S. Zhang, J. Yan, X. Huang, L. Wang, J. Gao, Interface sintering engineered superhydrophobic and durable nanofiber composite for high-performance electromagnetic interference shielding, J. Mater. Sci. Technol. 98 (2022) 62–71.
[24] J. Luo, S. Gao, H. Luo, L. Wang, X. Huang, Z. Guo, X. Lai, L. Lin, R.K.Y. Li, J. Gao, Superhydrophobic and breathable smart MXene-based textile for multifunctional wearable sensing electronics, Chem. Eng. J. 406 (2021) 126898.
[25] M. Amjadi, K. Kyung, I. Park, M. Sitti, Stretchable, skin-mountable, and wearable strain sensors and their potential applications: a review, Adv. Funct. Mater. 26 (2016) 1678–1698.
[26] Y. Fu, Y. Li, Y. Liu, P. Huang, N. Hu, S. Fu, High-performance structural flexible strain sensors based on graphene-coated glass fabric/silicone composite, ACS Appl. Mater. Interfaces 10 (2018) 35503–35509.
[27] S. Wang, Y. Fang, H. He, L. Zhang, C. Li, J. Ouyang, Wearable stretchable dry and self-adhesive strain sensors with conformal contact to skin for high-quality motion monitoring, Adv. Funct. Mater. (2020) 2007495.
[28] O. Redondo, S.G. Prolongo, M. Campo, C. Sbarufatti, M. Giglio, Anti-icing and de-icing coatings based Joule's heating of graphene nanoplatelets, Compos. Sci. Technol. 164 (2018) 65–73.
[29] A. Doblas, G.D. Rosario, M.G. Prolongo, S.G. Prolongo, Electric heating performance of nanodoped polyurethane coatings, Prog. Org. Coat. 135 (2019) 185–190.
[30] A. Cortés, X.F.S. Romate, A. Jiménez-Suárez, M. Campo, M.G. Prolongo, A. Ureña, S.G. Prolongo, 3D printed anti-icing and de-icing system based on CNT/GNP doped epoxy composites with self-curing and structural health monitoring capabilities, Smart Mater. Struct. 30 (2020), 025016.
[31] A. Cortés, A. Jiménez-Suárez, M. Campo, A. Ureña, S.G. Prolongo, 3D printed epoxy-CNTs/GNPs conductive inks with application in anti-icing and de-icing systems, Eur. Polym. J. 141 (2020) 110090.
[32] S. Suñer, R. Joffe, J.L. Tipper, N. Emami, Ultra high molecular weight polyethylene/graphene oxide nanocomposites: thermal, mechanical and wettability characterisation, Compos. Part B 78 (2015) 185–191.
[33] J. Gao, J. Luo, L. Wang, X. Huang, H. Wang, X. Song, M. Hu, L. Tang, H. Xue, Flexible, superhydrophobic and highly conductive composite based on non-woven polypropylene fabric for electromagnetic interference shielding, Chem. Eng. J. 364 (2019) 493–502.
[34] L. Wu, J. Luo, Y. Li, W. Zhang, L. Wang, X. Huang, W. Xiao, L. Tang, J. Gao, Emulsion dipping based superhydrophobic, temperature tolerant, and multifunctional coatings for smart strain sensing applications, Compos. Sci. Technol. 216 (2021) 109045.
[35] X.F. Sánchez-Romate, V. Saiz, A. Jiménez-Suárez, M. Campo, A. Ureña, The role of graphene interactions and geometry on thermal and electrical properties of epoxy nanocomposites: a theoretical to experimental approach, Polym. Test. 90 (2020) 106638.
[36] A. Kernin, K. Wan, Y. Liu, X. Shi, J. Kong, E. Bilotti, T. Peijs, H. Zhang, The effect of graphene network formation on the electrical, mechanical, and multifunctional properties of graphene/epoxy nanocomposites, Compos. Sci. Technol. 169 (2019) 224–231.
[37] A.O. Raji, T. Varadhachary, K. Nan, T. Wang, J. Lin, Y. Ji, B. Genorio, Y. Zhu, C. Kittrell, J.M. Tour, Composites of graphene nanoribbon stacks and epoxy for joule heating and deicing of surfaces, ACS Appl. Mater. Interfaces 8 (2016) 3551–3556.
[38] H. Kim, S. Lee, Characteristics of electrical heating elements coated with graphene nanocomposite on polyester fabric: effect of different graphene contents and annealing temperatures, Fibers Polym. 19 (2018) 965–976.
[39] R. Moriche, M. Sanchez, S.G. Prolongo, A. Jimenez-Suarez, A. Urena, Reversible phenomena and failure localization in self-monitoring GNP/epoxy nanocomposites, Compos. Struct. 136 (2016) 101–105.
[40] W. Li, Y. Zhou, Y. Wang, L. Jiang, J. Ma, S. Chen, F. Zhou, Core–sheath fiber-based wearable strain sensor with high Stretchability and sensitivity for detecting human motion, Adv. Electron. Mater. 7 (2021) 2000865.
[41] I.S. Bayer, Mechanisms of surface icing and deicing technologies, ice adhesion: mechanism, Meas. Mitig. (2020) 325–359.